ACS Sustainable Chemistry & Engineering

pubs.acs.org/journal/ascecg

Research Article

Supported Bifunctional Molybdenum Oxide-Palladium Catalysts for Selective Hydrodeoxygenation of Biomass-Derived Polyols and 1,4-Anhydroerythritol

Sandra Albarracin-Suazo, Lucas Freitas de Lima e Freitas, Blake MacQueen, Andreas Heyden, Jochen A. Lauterbach, Eranda Nikolla,* and Yomaira J. Pagán-Torres*

Cite This: https://doi.org/10.1021/acssuschemeng.1c06877

Read Online

ACCESS | Metrics & More | Article Recommendations | Supporting Information

ABSTRACT: Selective removal of oxygen from biomass-derived polyols is critical toward bridging the gap between biomass feedstocks and the production of commodity chemicals. In this work, we show that earth-abundant molybdenum oxide based heterogeneous catalysts are active, selective, and stable for the cleavage of vicinal C−O bonds in biomass-derived polyols. Catalyst characterization (Raman spectroscopy, X-ray photoelectron spectroscopy (XPS), diffuse reflectance infrared Fourier transform spectroscopy (DRIFTS)) shows that partially reduced MoO_x centers are responsible for C−O bond cleavage and are generated *in situ* by hydrogen dissociated atoms over palladium (Pd) nanoparticles. We find that the support, TiO_2, facilitates communication between the hydrogen dissociating metal and dispersed MoO_x sites through hydrogen spillover. Reactivity studies using a biomass-derived model substrate (1,4-anhydroerythritol) show the effective removal of vicinal hydroxyls over MoO_x-Pd/TiO_2 producing tetrahydrofuran with >98% selectivity at 29% conversion. Catalyst stability is demonstrated upon cycling. These studies are critical toward the development of low-cost heterogeneous catalysts for sustainable hydrodeoxygenation of biobased polyols to platform chemicals.

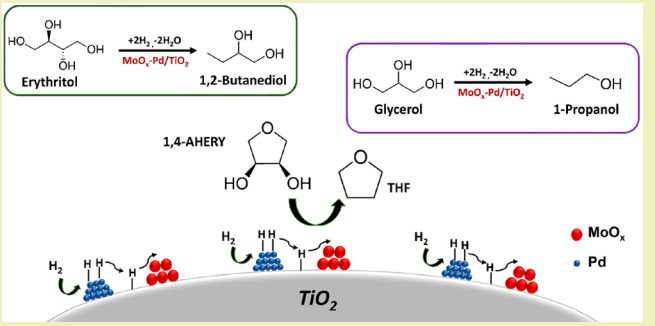

KEYWORDS: *Biomass conversion, Hydrodeoxygenation, Molybdenum, Polyols, Selective Catalysis, Glycerol, Deoxydehydration*

INTRODUCTION

Developing pathways to convert lignocellulosic biomass to chemicals and fuels is crucial to addressing concerns associated with increasing trends in global climate change and the depletion of nonrenewable carbon-based feedstocks (e.g., petroleum).[1−7] Although lignocellulosic biomass serves as a renewable carbon source to produce chemicals (e.g., alcohols, furans, diols), the high O/C ratio of biomass-derived compounds (e.g., sugars, sugar alcohols) requires the development of catalysts that can selectively and partially remove oxygen functionalities by hydrodeoxygenation (HDO) reactions.[8−10] An example of HDO chemistries, which has evolved into an efficient alternative to produce chemical building blocks (e.g., 1,4-butanediol (1,4-BDO), and 1,2-butanediol (1,2-BDO)) with applications in the polymer industry is the removal of vicinal hydroxyls from biomass-derived polyols (glycerol and erythritol) and cyclic molecules (e.g., 1,4-anhydroerythritol (1,4-AHERY)) by sequential deoxydehydration (DODH) and hydrogenation reactions (also referred to as simultaneous HDO, Scheme 1).[11−14] Erythritol is a C_4-polyol produced in high yields from the commercial fermentation of glucose and sucrose, and 1,4-AHERY is a molecule with *cis*-vicinal hydroxyls which can be produced from the simple dehydration of erythritol.[15,16]

Various heterogeneous catalysts have been reported for the simultaneous HDO of polyols and cyclic ethers. The catalysts are comprised of supported oxophilic metals (e.g., ReO_x, WO_x) promoted by noble metals (e.g., Ir, Pd, Rh).[11,17−27] Recently, studies have demonstrated the removal of hydroxyls from erythritol over Ir-ReO_x/SiO_2, Ir-ReO_x/TiO_2, Pt-WO_x/SiO_2, and ReO_x-Pd/CeO_2, mainly producing monomer building blocks, such as 1,2-BDO, 1,4-BDO, and 1,3-butanediol (1,3-BDO).[12,13,15,18,19] Furthermore, the single-step transformation of vicinal hydroxyls in 1,4-AHERY to the corresponding alkene (2,5-dihydrofuran (2,5-DHF)) by DODH has been demonstrated over supported ReO_x.[28] Researchers have also demonstrate that the addition of Pd to ReO_x supported on

Received: October 8, 2021
Revised: April 14, 2022

Scheme 1. Simultaneous Hydrodeoxygenation (Deoxydehydration + Hydrogenation) of Biomass-Derived Polyols and Cyclic Molecules

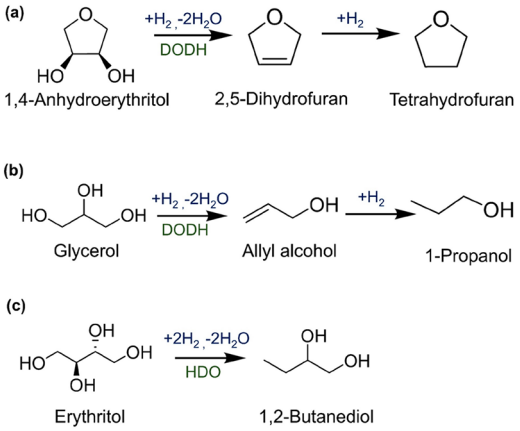

CeO_2 leads to conversion of 1,4-AHERY to tetrahydrofuran (THF) at 413 K and a hydrogen pressure of 80 bar with 99% selectivity at 38% conversion by simultaneous HDO.[12,13] On the basis of kinetic and computational studies, the active sites proposed for the ReO_x-Pd/CeO_2 were isolated Re^{4+} species formed by the reduction of Re^{6+} species in the presence of Pd-dissociated hydrogen atoms.[12,13] There has been spectroscopic evidence that the ReO_x exists in a mono-oxo (Re═O) and a dioxo (O═Re═O) state on the ReO_x-Pd/CeO_2 catalyst, which further supports the proposed active sites.[29] The reported catalytic cycle for simultaneous HDO of 1,4-AHERY involves the coordination of vicinal hydroxyls of the substrate to Re^{4+} centers to form a diolate, followed by C−O bond scission and the hydrogenation of the C═C to form THF.[13]

Despite high activities and product yields that have been reported for removing vicinal hydroxyls from polyols and cyclic ethers, the development of economically viable processes with high-cost Re catalysts remains challenging.[30] An alternative redox-active metal with similar properties to Re is molybdenum (Mo).[31,32] We have recently shown via density functional theory (DFT) calculations that supported monomeric MoO_x on TiO_2 is effective at C−O bond cleavage of 1,4-AHERY by DODH to produce 2,5-DHF.[28] We have also shown that MoO_x coupled with Pd on TiO_2 can catalyze the HDO of biomass-derived substrates containing carboxylic acid moieties, such as tartaric acid to produce succinic acid.[33] These studies showcase the flexibility of supported MoO_x species in a reducing environment to selectively cleave C−O bonds in substrates with multiple functional groups.

In this study, we demonstrate the HDO of 1,4-AHERY and polyols (glycerol and erythritol) using a MoO_X and Pd supported on TiO_2 (MoO_X-Pd/TiO_2) catalyst with high catalytic activity and selectivity toward vicinal diol cleavage under mild reaction conditions (413 K and hydrogen pressure of 52 bar). In addition, the catalyst shows remarkable catalytic stability upon multiple reuse cycles. We show that MoO_X-Pd/TiO_2 outperforms other supported catalysts with varying combinations of noble metals (Rh, Pt, Pd) and redox metal oxide centers (ReO_x, WO_x, MoO_x) for simultaneous removal of vicinal hydroxyls from 1,4-AHERY. Detailed catalyst characterization studies using Raman spectroscopy, X-ray photoelectron spectroscopy (XPS), diffuse reflectance infrared Fourier transform spectroscopy (DRIFTS), and X-ray diffraction (XRD) were conducted to discern the nature of the catalyst active site and postulate a plausible reaction mechanism for the HDO of 1,4-AHERY over MoO_X-Pd/TiO_2. These studies significantly impact the development of stable catalytic materials comprised of earth-abundant oxophillic metals (i.e., molybdenum) for deoxygenation of biomass-derived polyols with vicinal hydroxyl groups.

EXPERIMENTAL SECTION

Materials. All commercial materials were used as received. $(NH_4)_6Mo_7O_{24}\cdot 4H_2O$, $Pd(NO_3)_2\cdot 2H_2O$, NH_4ReO_4, $H_2PtCl_6\cdot 6H_2O$, $RhCl_3\cdot xH_2O$, ZrO_2, and pyridine (>99%) were purchased from Sigma-Aldrich. TiO_2 (P25-Acros Organics), $(NH_4)_{10}W_{12}O_{41}\cdot xH_2O$, 1,4-anhydroerythritol (>98%), erythritol (99%), glycerol (>99.5%), and 1,4-dioxane (>99%) were purchased from Fisher Scientific. SiO_2 (Cab-o-sil EH-5 fumed silica) was obtained from Cabot Corporation. γ-Al_2O_3 was purchased from STREM.

Catalyst Synthesis. Monometallic catalysts MoO_x/TiO_2 (2 wt % Mo) and Pd/TiO_2 (0.3 wt % Pd) were prepared by incipient wetness impregnation of aqueous solutions of $(NH_4)_6Mo_7O_{24}\cdot 4H_2O$ and $Pd(NO_3)_2\cdot 2H_2O$ on TiO_2 (P25) as reported previously by Nacy et al.[33] Monometallic catalysts were then dried overnight at 393 K and calcined in air at 773 K for 3 h. The MoO_x-M/TiO_2 (2 wt % Mo, M/Mo molar ratio = 0.14) catalysts with varying hydrogen dissociating metal (M = Pd, Pt, Rh) were prepared by incipient wetness impregnation of aqueous solutions of $Pd(NO_3)_2\cdot 2H_2O$, $H_2PtCl_6\cdot 6H_2O$, and $RhCl_3\cdot xH_2O$ on TiO_2 (P25); followed by drying at 393 K for 12 h. The samples were then impregnated with an aqueous solution of $(NH_4)_6Mo_7O_{24}\cdot 4H_2O$, dried at 393 K for 12 h, and calcined in air at 773 K for 3 h. For supported catalyst M′O_x-Pd/TiO_2 (2 wt % M′, Pd/M′ molar ratio = 0.14) with varying oxophilic metals (M′ = Mo, Re, W), an aqueous solution of $Pd(NO_3)_2\cdot 2H_2O$ was deposited by incipient wetness on TiO_2 (P25), then dried at 393 K for 12 h. The dried powders were then impregnated with $(NH_4)_6Mo_7O_{24}\cdot 4H_2O$, NH_4ReO_4, and $(NH_4)_{10}W_{12}O_{41}\cdot xH_2O$; dried at 393 K for 12 h; and calcined in air at 773 K for 3 h. Catalysts with varying supports were prepared by incipient wetness impregnation of aqueous solutions of $Pd(NO_3)_2\cdot 2H_2O$ on TiO_2 (P25), ZrO_2, γ-Al_2O_3, and SiO_2. After drying the samples at 393 K for 12 h, an aqueous solution of $(NH_4)_6Mo_7O_{24}\cdot 4H_2O$ was deposited by incipient wetness impregnation prior to calcination in air at 773 K for 3 h. Metal loadings on the catalyst with varying supports was 0.3 wt % Pd and 2 wt % Mo.

Catalyst Activity and Selectivity Measurements. The HDO reactions were performed in a 50 mL high-pressure batch reactor (Parr Instrument, 4792-SS). For each HDO reaction, the desired amount of reactant (1,4-AHERY, erythritol, or glycerol), 1,4-dioxane, catalyst, and a magnetic stir bar were added to the batch reactor. After sealing the reactor, it was purged three times with N_2 and three additional times with H_2 to remove any residual air. The reactor was then pressurized with H_2 (21−72 bar), followed by heating to the desired reaction temperature (393−433 K), and stirring at 740 rpm. After the desired reaction time, the reactor was cooled by quenching in an ice−water bath. Post reaction, the catalyst was filtered, and the liquid products were quantified by high-performance liquid chromatography (HPLC, Waters Alliance e2695) and gas chromatography (GC, Agilent 7890B). Retention times and response factors for reactants and products were determined using commercial standards. The Waters HPLC was equipped with a Waters 2414 refractive index detector at 308 K and a Bio-Rad Aminex HPX-87H column (300 mm × 7.8 mm) operating at 303 K and a 0.005 M H_2SO_4 at a flow rate of 0.55 mL/min. HPLC analysis was conducted for the detection and quantification of erythritol and glycerol. The Agilent GC was equipped with a SHRXI-5MS capillary column (Shimadzu, 15 m × 0.53 mm ID × 0.25 μm) and flame ionization detector (FID, Agilent). GC analysis was used for the quantification of 1,4-AHERY, THF, 2,5-DHF, 2,3-dihydrofuran (2,3-DHF), 1,2-BDO, 1,4-BDO, 2,3-BDO, 1,3-propanediol, 1,2-propanediol, 1-propanol, 2-propanol, propanal,

https://doi.org/10.1021/acssuschemeng.1c06877
ACS Sustainable Chem. Eng. XXXX, XXX, XXX−XXX

Table 1. Hydrodeoxygenation of 1,4-AHERY over Supported Bifunctional Catalysts Composed of Redox Metal Oxides Coupled with Hydrogen Dissociating Metals[a]

			product selectivity (%)						
entry	catalyst	conv. (%)	THF	2,5-DHF	2,3-DHF	1,2-BDO	1,4-BDO	THF formation rate ($\times 10^{-5}$ mol g_{cat}^{-1} min^{-1})	THF formation rate (mol mol_{co}^{-1} min^{-1})[b]
1	MoO_X-Pd/TiO_2	29	>98	<1	<1			1.79 ± 0.11	0.22
2	MoO_X-Pt/TiO_2	28	81		<1		4	1.40 ± 0.06	0.17
3	MoO_X-Rh/TiO_2	29	46	6	3		10	0.83 ± 0.09	0.12
4	ReO_X-Pd/TiO_2	26	40	<1	<1		3	0.68 ± 0.06	0.04
5	WO_X-Pd/TiO_2	<1	25			6	6	0.003 ± 0.0002	0.0006
6	MoO_X-Pd/ZrO_2	2	94					0.09 ± 0.01	0.02
7	MoO_X-Pd/SiO_2	<1	41	48				0.008 ± 0.0003	0.003
8	MoO_X-Pd/Al_2O_3	<1						~0	~0
9	MoO_x/TiO_2	<1						~0	~0
10	Pd/TiO_2	~0						~0	~0
11	TiO_2	~0						~0	~0

[a]Reaction conditions: 1,4-AHERY (5 mmol), 1,4-dioxane (24 mL), catalyst (160 mg), H_2 pressure (52 bar), 413 K, reaction time (8 h). Metal loadings for M′O_x-M/support (2 wt % M′ = Mo, Re, W; M = Pd, Pt, Rh; M/M′ molar ratio = 0.14). [b]THF formation rates are normalized by total CO uptake measurements (Table S2).

and allyl alcohol. The following equations were used to determine conversions of different substrates (i) and product selectivity:

$$\text{conversion of reactant } i\ [\%] = \frac{(\text{initial moles reactant}_i) - (\text{final moles of reactant}_i)}{\text{initial moles reactant}_i} \times 100 \quad (1)$$

$$\text{product } n \text{ selectivity}[\%] = \frac{\text{final moles of product}_n}{(\text{initial moles of reactant}_i) - (\text{final moles of reactant}_i)} \times 100 \quad (2)$$

Error bars reported for product formation rates were calculated from the standard deviation of a minimum of three independent reaction runs.

Catalyst Stability Measurements. MoO_x-Pd/TiO_2 recycling studies were carried out following the reaction protocol described above. After the 1,4-AHERY HDO reaction, the catalyst was recovered using vacuum filtration and washed with 1,4-dioxane. The recovered catalysts were then dried at 393 K for 12 h and calcined at 773 K for reuse in subsequent HDO reaction runs.

Catalyst Characterization. Elemental analysis of Pd and Mo loadings for fresh and spent MoO_x-Pd/TiO_2 was conducted using inductively coupled plasma optical emission spectroscopy (ICP-OES) performed by Galbraith Laboratories, Inc. (2323 Sycamore Drive, Knoxville, TN, 37921). Surface area measurements were performed using a Micrometrics ASAP 2020 instrument. The surface area was determined at liquid nitrogen temperature (77 K) using the Brunauer–Emmett–Teller (BET) analysis (Table S1). Each sample was degassed at 423 K for 12 h under vacuum to remove moisture prior to the surface area measurements.

CO (Airgas, UHP) uptake experiments of the catalysts were performed in a Micromeritics ASAP 2020 instrument at 308 K. Typically, 0.1 g of the sample (<125 mm particle size) was pressed into a pellet. The pellet was placed in the analysis cell, and it was then dried under vacuum (<5 μmHg) for 0.5 h at 373 K. The pellet was treated in O_2 at 623 K for 0.5 h, followed by degassing (<5 μmHg) at 623 K for 0.5 h. The samples were then reduced in a H_2 flow at 673 K for 2 h, degassed (<5 μmHg) at 673 K for 2 h, and finally cooled to 308 K. The adsorption isotherm measurement was performed by exposing the catalyst to CO (between 100 and 450 mmHg).

Powder XRD analysis of TiO_2, Pd/TiO_2, MoO_x/TiO_2, and MoO_x-Pd/TiO_2 was conducted with a Rigaku MiniFlex II, which utilized a Cu Kα source of radiation (α = 1.5406). XRD patterns were recorded from a 2θ of 10°–80° at a rate of 2°/min. Raman experiments were carried out with a Horiba XploRA Plus Raman microscope instrument. The excitation source was a 30 mW, 638 nm solid-state laser, which was calibrated using a polystyrene standard. The resulting scattered light was detected using a HORIBA Scientific charge-coupled device detector. The detector was thermoelectrically cooled to 223 K during experimentation. All spectra were taken under ambient conditions with the 50× objective, a grating of 1800 (450–850 nm), and a filter of 25% laser power. All Raman spectra were normalized to the TiO_2 E_g mode peak intensity, which was located at roughly 640 cm^{-1}. XPS surface analysis of the powder catalysts was conducted on a ThermoScientific Nexsa XPS System with a monochromatic Al Kα source operated at 50 eV with a step size of 0.1 eV and a 100 ms dwell time for Mo 3d and recorded using 50 scans, employing a hemispherical analyzer. Analysis of the data was carried out using CasaXPS software, and the synthetic line-shape (Shirley) and the corresponding relative sensitive factor (RSF, Al-Scofield) were used to determine the relative region quantification. The correction was accomplished by shifting the C 1s peak as a reference at 284.8 eV.

FTIR experiments were performed with a ThermoFisher Nicolet iS10 FTIR spectrometer equipped with an MCT detector. A high-temperature reaction chamber (Harrick Scientific) was loaded with approximately 100 mg of a mixture of the catalyst (<38 μm particle size) with IR-grade KBr powder (<38 μm, Sigma-Aldrich) at a 1:5 weight ratio. The samples were treated at 623 K under a helium flow for 1 h to remove moisture. The samples were then cooled down to 413 K and treated with a flow of 5% H_2/Ar for 1 h. After reduction, the chamber was purged with helium for 1 h and cooled down to 303 K. Background spectra were recorded at 303 and 413 K. Pyridine stored in a bubbler was then flowed over the sample using He as the carrier gas. The sample was then purged with He while heating to 423 K. The He flow was held at 423 K for 1 h to remove any additional physisorbed pyridine. Spectra were then collected at 303 and 413 K using 100 scans and 4 cm^{-1} resolution in the wavelength range from 1300 to 1700 cm^{-1}. The data collected was in Kubelka–Munk units. For FTIR experiments containing water vapor, He flowing through a water saturator at 303 K was introduced to catalyst samples after reduction and cooling. The chamber was then purged with He at 423 K to remove any excess water before collection of the background spectrum at 303 and 413 K.

RESULTS AND DISCUSSION

Reactivity Studies of Supported Bifunctional Catalysts for 1,4-AHERY HDO to THF. The catalytic activity and product selectivity of supported catalysts containing an oxophilic metal (i.e., Mo, Re, W) and a hydrogen dissociating

https://doi.org/10.1021/acssuschemeng.1c06877
ACS Sustainable Chem. Eng. XXXX, XXX, XXX–XXX

metal (i.e., Pt, Pd, Rh) on simultaneous HDO (DODH +hydrogenation) of 1,4-AHERY to THF at 413 K and 52 bar of H_2 are reported in Table 1. Initially, the performance of MoO_x/TiO_2 promoted by hydrogen dissociating metals (Pd, Pt, Rh) was evaluated on the cleavage of vicinal diols from 1,4-AHERY, Table 1 (entries 1−3). The rates were normalized by catalyst CO uptake measurements (Table S2) and by noble metal content (Table S3). The addition of Pd to MoO_x/TiO_2 resulted in the highest THF formation rate (0.22 mol·mol_{co}^{-1} · min^{-1}) and THF selectivity (>98% at 29% conversion of 1,4-AHERY) among the hydrogen dissociating metals studied. In comparison, MoO_x/TiO_2 promoted by Pt resulted in similar HDO activity but lower THF selectivity (81%) at 28% conversion of 1,4-AHERY and THF formation rate (0.17 mol·mol_{co}^{-1} ·min^{-1}). For Rh supported on MoO_x/TiO_2, THF was produced along with other reaction intermediates (i.e., 2,5-DHF, 2,3-DHF, and 1,4-BDO) at similar 1,4-AHERY conversions. Hydrogen dissociating properties of supported Pt and Rh particles have been demonstrated in the literature;[17] however, supported oxophilic metals promoted by Rh and Pt have also been reported to catalyze ring-opening reactions of biomass-derived cyclic ethers.[10,34,35] Since Pd showed no activity in 1,4-AHERY ring-opening under the HDO reaction conditions studied, Pd was selected as the hydrogen dissociating metal to study the effect of supported oxophilic metal centers (MoO_x, ReO_x, WO_x) on 1,4-AHERY HDO. Among the oxophilic metal centers considered, MoO_x in MoO_x-Pd/TiO_2 (Table 1, entry 1) showed the highest THF formation rates and selectivity compared to ReO_x-Pd/TiO_2 and WO_x-Pd/TiO_2.

Recently, studies have demonstrated that the activity of multifunctional polyol HDO catalysts containing oxophilic metals (e.g., ReO_x) and metallic sites (e.g., Ir) can be affected by the redox and acidic properties of catalyst supports.[24] The effect of the support was studied by varying the TiO_2 support to ZrO_2, SiO_2, and Al_2O_3 as shown in Table 1, entries 1 and 6−8. TiO_2 supported MoO_X-Pd gave the highest THF rate of formation (0.22 mol·mol_{co}^{-1} ·min^{-1}) and THF selectivity compared to MoO_X-Pd supported on ZrO_2, Al_2O_3, and SiO_2. MoO_X-Pd/Al_2O_3 and MoO_X-Pd/SiO_2 exhibited the lowest 1,4-AHERY HDO activity (<1% conversion). The support-dependent performance is consistent with the highest rates of proton transport on reducible oxides (i.e., TiO_2), facilitating communication between activated hydrogen atoms over Pd and the redox metal (MoO_x).[36] Overall, these reactivity studies indicate that MoO_x and Pd supported on TiO_2 is the optimal catalyst among the ones considered for vicinal diol cleavage of 1,4-AHERY to THF. The control systems, monometallic catalysts (MoO_x/TiO_2 and Pd/TiO_2), and bare TiO_2 exhibited insignificant HDO activity, indicating all three components were necessary for selective conversion of 1,4-AHERY to THF, Table 1, entries 9−11.

The effect of the Pd/Mo molar ratio (0.07−0.45) for a fixed Mo loading (2 wt %) on TiO_2 was evaluated for 1,4-AHERY HDO. As shown in Figure S1, the 1,4-AHERY conversion goes through a maximum of 29% for a Pd/Mo ratio of 0.14 with >98% selectivity to THF. For the 0.07, 0.27, and 0.45 Pd/Mo molar ratios, the conversion and THF selectivity decrease for equivalent reaction times. Literature studies have demonstrated that the structure of supported MoO_x species can be tailored between isolated, oligomeric, and polymeric based on the loading of Mo, consequently impacting catalyst activity and selectivity in HDO reactions.[37] To probe this effect, the Mo loading was varied in MoO_X-Pd/TiO_2 while leaving the molar ratio of Pd/Mo = 0.14, as shown in Figure S2. The 1,4-AHERY conversion increased from 10% for 0.5 wt % Mo to 34% for 4 wt % Mo, whereas a decrease in conversion was observed at higher Mo loadings. This is consistent with the formation of polymeric MoO_x species at higher loadings as evidenced by Raman. Although MoO_X-Pd/TiO_2 with 4 wt % Mo showed the highest catalyst conversion (34%), THF selectivity (92%) was lower than the catalyst with 2 wt % Mo loading (>98% THF selectivity) at a slightly lower conversion (29%). Thus, the 2 wt % Mo and 0.3 wt % Pd supported on TiO_2 (Pd/Mo= 0.14) was selected to perform the kinetic and stability studies due to its high (>98%) selectivity to THF, while maintaining high activity with half of the Mo loading of the 4 wt % catalyst. The 2 wt % Mo and 0.3 wt % Pd supported on TiO_2 catalyst will be referred to as MoO_X-Pd/TiO_2 in the following sections.

To further understand the reaction pathway, a time-course study on 1,4-AHERY conversion over MoO_X-Pd/TiO_2 was performed (Figure S3). The reaction intermediates observed were 2,5-DHF and 2,3-DHF at times very close to zero (after the reactor reached the reaction temperature). Interestingly, 3-hydroxytetrahydrofuran was not observed as a reaction intermediate even at very low conversions (<10%), suggesting that OH removal was not sequential. However, this behavior is substrate-structure-dependent, since in our prior studies we showed that tartaric acid conversion over similar catalytic systems proceeded through sequential C−O bond cleavage.[33]

The effect of hydrogen pressure, reactant concentration, and temperature on the simultaneous HDO of 1,4-AHERY over MoO_X-Pd/TiO_2 was studied at 1,4-AHERY conversions <15%. The rate of THF formation as a function of hydrogen pressure was measured in the range of 21−72 bar, as shown in Figure 1a. The rate of THF formation with varying hydrogen pressure suggests an approximate first-order reaction dependence on hydrogen. Table S4 includes data on the hydrogen pressures

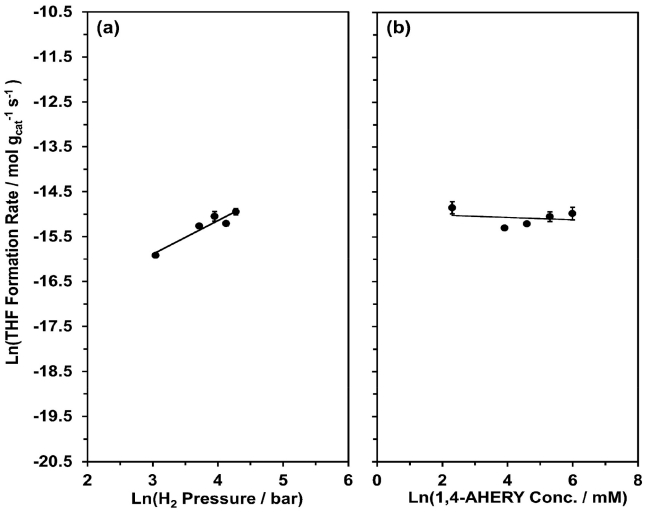

Figure 1. Effect of H_2 pressure and reactant concentration on the HDO of 1,4-AHERY to THF over MoO_x-Pd/TiO_2. (a) Reaction conditions: 1,4-AHERY (5 mmol), 1,4-dioxane (24 mL), H_2 pressure (21−72 bar), 413 K, catalyst (160 mg), metal loading on TiO_2 (2 wt % Mo, 0.3 wt % Pd). (b) Reaction conditions: 1,4-AHERY concentration in 1,4-dioxane (10−400 mM), H_2 pressure (52 bar), 413 K, catalyst (160 mg), metal loading on TiO_2 (2 wt % Mo, 0.3 wt % Pd). THF formation rates are reported for 1,4-AHERY conversions <15%.

https://doi.org/10.1021/acssuschemeng.1c06877
ACS Sustainable Chem. Eng. XXXX, XXX, XXX−XXX

evaluated and THF formation rates obtained for these experiments. The dependence of reactant concentration (10−400 mM of 1,4-AHERY in 1,4-dioxane) on the rate of THF formation was of zero order, indicating high coverage of the reactant on the active sites of MoO_X-Pd/TiO_2, Figure 1b. The 1,4-AHERY concentrations evaluated and THF formation rates obtained are reported in Table S5. From reaction rate measurements at temperatures between 393 and 433 K, an apparent energy barrier of 123 kJ mol^{-1} ± 11 kJ mol^{-1} was extracted. Table S6 shows the temperatures and THF formation rates used to determine the apparent activation energy barriers. The THF formation rates were obtained under differential reaction conditions with 1,4-AHERY conversions <15%.

The activity and selectivity of MoO_x-Pd/TiO_2 toward simultaneous HDO is not unique to 1,4-AHERY but is a characteristic of other substrates, such as C_3 and C_4 polyols. Table 2 shows that similar performances were achieved in the

Table 2. Hydrodeoxygenation of Polyols and 1,4-Anhydrothreitol over MoO_x-Pd/TiO_2[a]

substrate	conv. (%)	product selectivity (%)				
Erythritol	26	1,2-BDO (65)	1,4-BDO (21)	1,4-AHERY (7)	THF (7)	
Glycerol	12	1-Propanol (85)	Propanal (15)			
1,4-Anhydrothreitol	0					

[a]Reaction conditions: reactant (0.5 g), 1,4-dioxane (24 mL), catalyst (160 mg), H_2 pressure (52 bar), 413 K. Catalyst metal loading: Mo (2 wt %) and Pd (0.3 wt %) on TiO_2. Erythritol and 1,4-anhydrothreitol were run for 8 h, whereas glycerol was run for 6 h to obtain a wider product distribution.

HDO of vicinal hydroxyls for erythritol and glycerol. In the HDO of erythritol over MoO_x-Pd/TiO_2, the main product observed was 1,2-BDO, resulting from the removal of two vicinal hydroxyls. A time-course study on glycerol conversion over MoO_X-Pd/TiO_2 showed propanal as a reaction intermediate and 1-propanol as the main product even at low conversions (Figure S4). This suggests that C−O bond cleavage occurs over MoO_x sites, whereas isomerization of allyl alcohol (DODH product) to propanal and hydrogenation to 1-propanol is facilitated by Pd sites.[38−40] Interestingly, when 1,4-anhydrothreitol was reacted over MoO_x-Pd/TiO_2, no activity was observed, suggesting that the orientation of the hydroxyls was essential for the coordination of the substrate with the active site.

Catalyst Stability. The stability of the MoO_x-Pd/TiO_2 catalyst was evaluated over four reaction cycles, as shown in Figure 2. A 1,4-AHERY conversion of ∼29% and THF selectivity <98% were maintained after these cycles. The analysis of the Mo and Pd loading on the spent catalyst by ICP-OES showed no significant losses in Mo and Pd due to dissolution, Table S7. Furthermore, no significant variations in

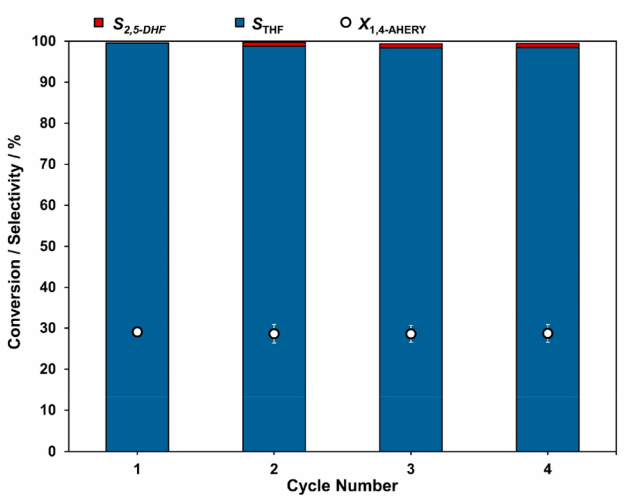

Figure 2. Catalyst stability in the HDO of 1,4-AHERY over MoO_x-Pd/TiO_2 (2 wt % Mo, 0.3 wt % Pd). Reaction conditions: 1,4-AHERY (5 mmol), 1,4-dioxane (24 mL), H_2 pressure (52 bar), 413 K, catalyst (160 mg), reaction time (8 h). Conversion (X) and selectivity (S).

CO chemisorption by the catalyst were observed before and after cycling, confirming its stability.

Insights on the Nature of MoO_X-Pd/TiO_2 Active Sites. Figure S5 shows the XRD patterns of as-synthesized MoO_x-Pd/TiO_2 (2 wt % Mo, 0.3 wt % Pd), MoO_X/TiO_2 (2 wt % Mo), Pd/TiO_2 (0.3 wt % Pd), and TiO_2. In all XRD patterns, only peaks corresponding to a mixture of rutile and anatase phases of TiO_2 were observed.[41] These results suggested that MoO_X and Pd sites were highly dispersed on the support and unable to be detected by XRD. Raman spectroscopy of MoO_x-Pd/TiO_2 was used to probe the antisymmetric (Mo−O−Mo) and terminal stretching (M═O) modes of dispersed MoO_x species at varying Mo loadings, Figure 3. For MoO_x-Pd/TiO_2 (0.5 wt % Mo, 0.1 wt % Pd), no bands associated with MoO_x species were observed due to the low Mo loading on the surface. For MoO_x/TiO_2 (2 wt % Mo), a Raman band located at 954 cm^{-1} corresponding to the terminal (Mo═O) stretching in isolated tetrahedra MoO_x species was observed.[42−44] With the addition of 0.3 wt % Pd to the

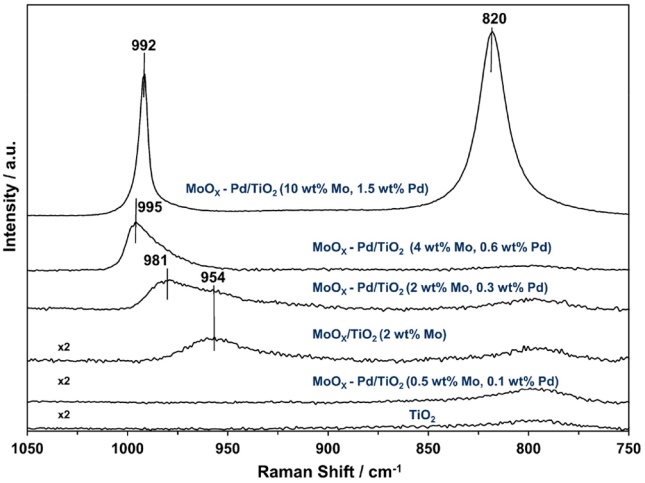

Figure 3. Raman spectra of TiO_2, MoO_x/TiO_2 (2 wt % Mo), and MoO_x-Pd/TiO_2 (0.5−10 wt % Mo, Pd/Mo molar ratio = 0.14).

https://doi.org/10.1021/acssuschemeng.1c06877
ACS Sustainable Chem. Eng. XXXX, XXX, XXX−XXX

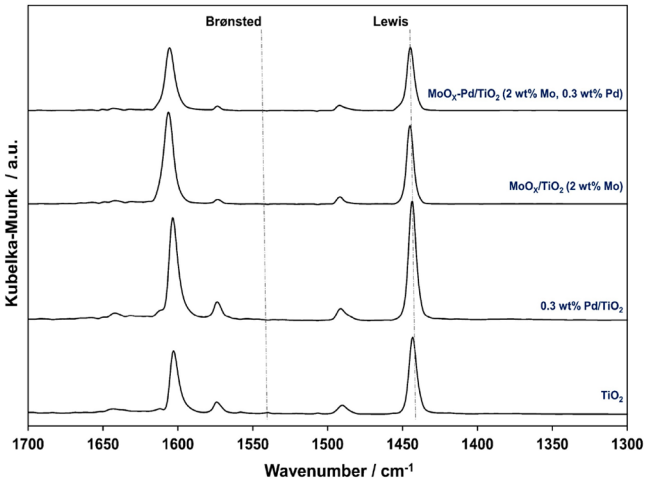

Figure 4. DRIFTS spectra of adsorbed pyridine on TiO_2, Pd/TiO_2 (0.3 wt % Pd), MoO_x/TiO_2 (2 wt % Mo), and MoO_x-Pd/TiO_2 (2 wt % Mo, 0.3 wt % Pd) after reduction at 413 K.

MoO_X/TiO_2, which led to the best performing catalyst, the deconvolution of the Raman spectra using a Gaussian band shape shows the appearance of a Raman band at 981 cm^{-1}, which is identified as terminal (Mo═O) stretching for oligomeric octahedral MoO_x species (Figure S6).[42−44] These results indicated that MoO_x-Pd/TiO_2 was comprised of a combination of both surface isolated tetrahedral and oligomeric octahedral MoO_x species. At Mo loadings >2 wt %, the Raman band shifted to 995 cm^{-1}, which correlated to the terminal (Mo═O) stretching mode of polymeric octahedral MoO_x species.[43] In the case of MoO_x-Pd/TiO_2 (10 wt % Mo, 1.5 wt % Pd), a monolayer formation of MoO_x species was observed as evidenced by the intense Raman bands at 820 and 992 cm^{-1} indicative of crystalline MoO_3.[43] This is consistent with the report by Wachs et al. which showed that a monolayer of Mo supported on TiO_2 was formed at ∼7 wt % Mo loadings.[44]

The Brønsted/Lewis acid properties of TiO_2, Pd/TiO_2 (0.3 wt % Pd), MoO_X/TiO_2 (2 wt % Mo), and MoO_x-Pd/TiO_2 (2 wt % Mo, 0.3 wt % Pd) were probed by pyridine FTIR studies on the catalysts after dehydration at 623 K and a reduction in hydrogen at 413 K, Figure 4. The ν_{19b} band for pyridine coordinated to Brønsted and Lewis acid sites at 1540 and 1450 cm^{-1}, respectively, were used to identify each type of site.[45,46] For all samples (TiO_2, Pd/TiO_2, MoO_x/TiO_2, and MoO_x-Pd/TiO_2), peaks at ∼1445 cm^{-1} and ∼1605 cm^{-1} were observed and attributed to the coordination of pyridine on Lewis acid sites. In the literature, C−O bond cleavage of polyols (e.g., glycerol) over catalysts comprised of oxophilic metals (e.g., WO_x, ReO_x) has been proposed to occur through Brønsted acid-catalyzed reactions.[10,47] However, in this case, pyridine FTIR spectra of MoO_x-Pd/TiO_2 (after reduction at 413 K) showed that no pyridine coordinated to Brønsted acid sites, suggesting that acid-catalyzed dehydration chemistry in the deoxygenation of 1,4-AHERY was limited over MoO_x-Pd/TiO_2. To evaluate the possible formation of Brønsted acid sites during reaction as a result of water formation, pyridine DRIFTS studies of Pd-MoO_x/TiO_2 after *in situ* reduction in hydrogen and exposure to water vapor were conducted. Figure S7 shows that the characteristic bands of Brønsted acidity were not observed for both untreated and treated Pd-MoO_x/TiO_2 with water vapor. These results suggested that even after exposure to water vapor the catalyst retained its Lewis acidic properties.

X-ray photoelectron spectroscopy was used to characterize changes in the oxidation state (electronic structure) of MoO_x species before (Figure 5a) and after 1,4-AHERY HDO (Figure 5b). A common feature of all of the catalysts with high selectivity to THF (i.e., MoO_x-Pd/TiO_2 (best performing), MoO_X-Pt/TiO_2, and MoO_X-Pd/ZrO_2) was the decrease in the oxidation state of Mo after reaction. This result clearly suggested that the selective site for C−O bond cleavage in 1,4-AHERY was a partially reduced MoO_x center, facilitated by hydrogen dissociated atoms over Pt or Pd. Although the spent catalysts were exposed to the environment prior to XPS analysis, hence the oxidation state of Mo was not exactly the same as under reaction conditions, our results clearly show that the reductive reaction conditions led to a decrease in the oxidation state of molybdenum. The extent of the reduced MoO_x species on the catalyst surface after reaction (MoO_x-Pd/TiO_2 > MoO_X-Pt/TiO_2 > MoO_X-Pd/ZrO_2) as determined by XPS directly correlated to the conversion of 1,4-AHERY on these catalysts. These studies indicated that the active catalytic

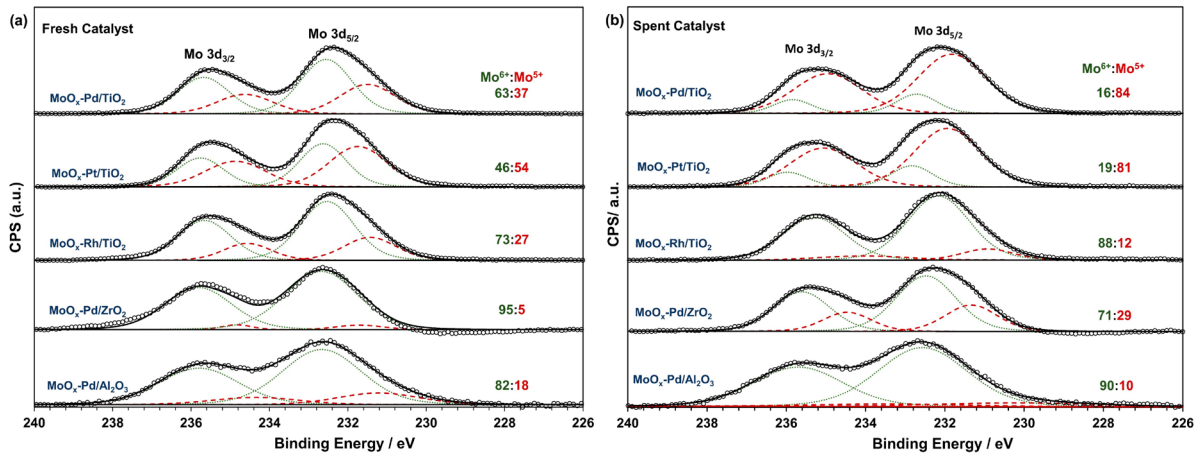

Figure 5. XPS spectra of the (3d) Mo energy region for (a) fresh and (b) spent MoO_x-Pd/TiO_2, MoO_x-Pt/TiO_2, MoO_x-Rh/TiO_2, MoO_x-Pd/ZrO_2, and MoO_x-Pd/Al_2O_3. Reaction conditions for spent catalyst: 1,4-AHERY (5 mmol), 1,4-dioxane (24 mL), catalyst (160 mg), H_2 pressure (52 bar), 413 K, reaction time (8 h).

https://doi.org/10.1021/acssuschemeng.1c06877
ACS Sustainable Chem. Eng. XXXX, XXX, XXX−XXX

sites for selective C−O bond activation in 1,4-AHERY were partially reduced MoO_x sites. Hence, possible sites for 1,4-AHERY HDO were unsaturated MoO_x sites by which C−O bonds were cleaved through an oxygen vacancy-driven mechanism.

Catalytic Cycle for 1,4-AHERY HDO over MoO_X-Pd/TiO_2. It is evident from the characterization discussed above that on the best performing MoO_X-Pd/TiO_2 catalyst, oxygen vacancies of MoO_x species are responsible for selective C−O bond cleavage in 1,4-AHERY. These vacancies are created *in situ* through hydrogen atoms generated on Pd. More specifically, a plausible catalytic cycle for simultaneous HDO (DODH+hydrogenation) of 1,4-AHERY over MoO_x-Pd/TiO_2 (2 wt % Mo, 0.3 wt % Pd) involves initial hydrogen dissociation over Pd nanoparticles followed by H_2 spillover and facile proton transfer on TiO_2, facilitating partial reduction of the MoO_x sites. This is followed by the adsorption and C−O bond cleavage of 1,4-AHERY on the oxygen vacancies of MoO_x to form 2,5-DHF. Given the low energy barrier expected for H_2 dissociation on Pd and transport on TiO_2,[36] the measured apparent activation energy barrier and the dependence of the rate on hydrogen are most likely associated with the reduction of the MoO_x sites leading to the generation of oxygen vacancies. Finally, the hydrogenation of the unsaturated carbon−carbon bond of 2,5-DHF to THF is catalyzed by the Pd sites.

CONCLUSIONS

The HDO of 1,4-AHERY to THF was studied over bifunctional catalysts comprised of a supported hydrogen dissociating metal center (Pd, Rh, Pt) coupled with a redox metal oxide center (MoO_x, ReO_x, WO_x). The catalyst resulting in the highest THF production rate (0.22 $mol{\cdot}mol_{co}^{-1}{\cdot}min^{-1}$) and selectivity (>98%) was a 2 wt % MoO_x-0.3 wt % Pd/TiO_2. Under optimized 1,4-AHERY HDO reaction conditions, the MoO_x-Pd/TiO_2 catalyst showed excellent stability upon cycling. Detailed reaction kinetics and characterization studies of MoO_x-Pd/TiO_2 suggested that direct cleavage of C−O bonds of 1,4-AHERY occurred over partially reduced Mo sites formed *in situ* through hydrogen dissociated atoms over Pd. These studies are critical toward development of an effective low-cost alternative to the state of the art HDO catalyst for the processing of biomass-based polyols.

ASSOCIATED CONTENT

Supporting Information

The Supporting Information is available free of charge at https://pubs.acs.org/doi/10.1021/acssuschemeng.1c06877.

Effect of MoO_x loading and Pd/Mo ratio on TiO_2 for 1,4-AHERY HDO, 1,4-AHERY and glycerol conversion over MoO_x-Pd/TiO_2 with time, elemental analysis of fresh and spent MoO_x-Pd/TiO_2, CO uptake measurements, XRD plots (MoO_x-Pd/TiO_2, Pd/TiO_2, MoO_x/TiO_2, TiO_2), Raman deconvolution spectra for MoO_x-Pd/TiO_2 (2 wt % Mo, 0.3 wt % Pd), DRIFTS of adsorbed pyridine over MoO_x-Pd/TiO_2 after water exposure, and kinetic studies data (PDF)

AUTHOR INFORMATION

Corresponding Authors

Yomaira J. Pagán-Torres − *Department of Chemical Engineering, University of Puerto Rico—Mayaguez Campus, Mayaguez, Puerto Rico 00681, United States;* orcid.org/0000-0002-8655-7058; Email: yomairaj.pagan@upr.edu

Eranda Nikolla − *Department of Chemical Engineering and Materials Science, Wayne State University, Detroit, Michigan 48202, United States;* orcid.org/0000-0002-8172-884X; Email: erandan@wayne.edu

Authors

Sandra Albarracin-Suazo − *Department of Chemical Engineering, University of Puerto Rico—Mayaguez Campus, Mayaguez, Puerto Rico 00681, United States*

Lucas Freitas de Lima e Freitas − *Department of Chemical Engineering and Materials Science, Wayne State University, Detroit, Michigan 48202, United States;* orcid.org/0000-0002-8730-8045

Blake MacQueen − *Department of Chemical Engineering, University of South Carolina, Columbia, South Carolina 29208, United States*

Andreas Heyden − *Department of Chemical Engineering, University of South Carolina, Columbia, South Carolina 29208, United States;* orcid.org/0000-0002-4939-7489

Jochen A. Lauterbach − *Department of Chemical Engineering, University of South Carolina, Columbia, South Carolina 29208, United States;* orcid.org/0000-0001-8303-7703

Complete contact information is available at: https://pubs.acs.org/10.1021/acssuschemeng.1c06877

Notes

The authors declare no competing financial interest.

ACKNOWLEDGMENTS

We gratefully acknowledge financial support from the National Science Foundation (OIA-1632824). L.F.L.F. and E.N. gratefully acknowledge financial support from the National Science Foundation for funding this research through CHE Grant No. 1900176. The authors also thank the Lumigen Instrument Center at Wayne State University for the use of the X-ray diffraction/spectroscopy (National Science Foundation MRI-1427926, MRI-1849578).

REFERENCES

(1) Chheda, J. N.; Huber, G. W.; Dumesic, J. A. Liquid-Phase Catalytic Processing of Biomass-Derived Oxygenated Hydrocarbons to Fuels and Chemicals. *Angew. Chem., Int. Ed.* **2007**, *46* (38), 7164−7183.

(2) Alonso, D. M.; Wettstein, S. G.; Dumesic, J. A. Bimetallic catalysts for upgrading of biomass to fuels and chemicals. *Chem. Soc. Rev.* **2012**, *41* (24), 8075−8098.

(3) Serrano-Ruiz, J. C.; West, R. M.; Dumesic, J. A. Catalytic Conversion of Renewable Biomass Resources to Fuels and Chemicals. *Annu. Rev. Chem. Biomol. Eng.* **2010**, *1* (1), 79−100.

(4) Peters, G. P.; Andrew, R. M.; Canadell, J. G.; Friedlingstein, P.; Jackson, R. B.; Korsbakken, J. I.; Le Quéré, C.; Peregon, A. Carbon dioxide emissions continue to grow amidst slowly emerging climate policies. *Nat. Clim. Change.* **2020**, *10* (1), 3−6.

(5) Corma, A.; Iborra, S.; Velty, A. Chemical routes for the transformation of biomass into chemicals. *Chem. Rev.* **2007**, *107*, 2411−2502.

(6) Balakrishnan, M.; Sacia, E. R.; Sreekumar, S.; Gunbas, G.; Gokhale, A. A.; Scown, C. D.; Toste, F. D.; Bell, A. T. Novel pathways for fuels and lubricants from biomass optimized using life-cycle greenhouse gas assessment. *Proc. Natl. Acad. Sci. U.S.A.* **2015**, *112* (25), 7645−7649.

(7) Alonso, D. M.; Hakim, S. H.; Zhou, S.; Won, W.; Hosseinaei, O.; Tao, J.; Garcia-Negron, V.; Motagamwala, A. H.; Mellmer, M. A.;

Huang, K.; Houtman, C. J.; Labbé, N.; Harper, D. P.; Maravelias, C. T.; Runge, T.; Dumesic, J. A. Increasing the revenue from lignocellulosic biomass: Maximizing feedstock utilization. *Sci. Adv.* **2017**, *3*, 1−7.
(8) Robinson, A. M.; Hensley, J. E.; Medlin, J. W. Bifunctional Catalysts for Upgrading of Biomass-Derived Oxygenates: A Review. *ACS Catal.* **2016**, *6* (8), 5026−5043.
(9) Kim, S.; Kwon, E. E.; Kim, Y. T.; Jung, S.; Kim, H. J.; Huber, G. W.; Lee, J. Recent advances in hydrodeoxygenation of biomass-derived oxygenates over heterogeneous catalysts. *Green Chem.* **2019**, *21* (14), 3715−3743.
(10) Yun, Y. S.; Berdugo-Díaz, C. E.; Flaherty, D. W. Advances in Understanding the Selective Hydrogenolysis of Biomass Derivatives. *ACS Catal.* **2021**, *11* (17), 11193−11232.
(11) Amada, Y.; Watanabe, H.; Hirai, Y.; Kajikawa, Y.; Nakagawa, Y.; Tomishige, K. Production of Biobutanediols by the Hydrogenolysis of Erythritol. *ChemSusChem* **2012**, *5* (10), 1991−1999.
(12) Ota, N.; Tamura, M.; Nakagawa, Y.; Okumura, K.; Tomishige, K. Hydrodeoxygenation of vicinal OH groups over heterogeneous rhenium catalyst promoted by palladium and ceria support. *Angew. Chem., Int. Ed.* **2015**, *54*, 1897−1900.
(13) Ota, N.; Tamura, M.; Nakagawa, Y.; Okumura, K.; Tomishige, K. Performance, Structure, and Mechanism of ReOx-Pd/CeO2 Catalyst for Simultaneous Removal of Vicinal OH Groups with H2. *ACS Catal.* **2016**, *6*, 3213−3226.
(14) Tomishige, K.; Nakagawa, Y.; Tamura, M. Selective hydrogenolysis and hydrogenation using metal catalysts directly modified with metal oxide species. *Green Chem.* **2017**, *19*, 2876−2924.
(15) Nakagawa, Y.; Kasumi, T.; Ogihara, J.; Tamura, M.; Arai, T.; Tomishige, K. Erythritol: Another C4 Platform Chemical in Biomass Refinery. *ACS Omega* **2020**, *5* (6), 2520−2530.
(16) Jeya, M.; Lee, K.-M.; Tiwari, M. K.; Kim, J.-S.; Gunasekaran, P.; Kim, S.-Y.; Kim, I.-W.; Lee, J.-K. Isolation of a novel high erythritol-producing Pseudozyma tsukubaensis and scale-up of erythritol fermentation to industrial level. *Appl. Microbiol. Biotechnol.* **2009**, *83* (2), 225−231.
(17) Said, A.; Da Silva Perez, D.; Perret, N.; Pinel, C.; Besson, M. Selective C−O Hydrogenolysis of Erythritol over Supported Rh-ReOx Catalysts in the Aqueous Phase. *ChemCatChem.* **2017**, *9* (14), 2768−2783.
(18) Gu, M.; Liu, L.; Nakagawa, Y.; Li, C.; Tamura, M.; Shen, Z.; Zhou, X.; Zhang, Y.; Tomishige, K. Selective Hydrogenolysis of Erythritol over Ir−ReOx/Rutile-TiO2 Catalyst. *ChemSusChem* **2021**, *14* (2), 642−654.
(19) Liu, L.; Cao, J.; Nakagawa, Y.; Betchaku, M.; Tamura, M.; Yabushita, M.; Tomishige, K. Hydrodeoxygenation of C4−C6 sugar alcohols to diols or mono-alcohols with the retention of the carbon chain over a silica-supported tungsten oxide-modified platinum catalyst. *Green Chem.* **2021**, *23* (15), 5665−5679.
(20) Liu, L.; Kawakami, S.; Nakagawa, Y.; Tamura, M.; Tomishige, K. Highly active iridium−rhenium catalyst condensed on silica support for hydrogenolysis of glycerol to 1,3-propanediol. *Appl. Catal., B* **2019**, *256*, 117775.
(21) Liu, L.; Asano, T.; Nakagawa, Y.; Gu, M.; Li, C.; Tamura, M.; Tomishige, K. Structure and performance relationship of silica-supported platinum-tungsten catalysts in selective C-O hydrogenolysis of glycerol and 1,4-anhydroerythritol. *Appl. Catal., B* **2021**, *292*, 120164.
(22) Stephens, K. J.; Allgeier, A. M.; Bell, A. L.; Carlson, T. R.; Cheng, Y.; Douglas, J. T.; Howe, L. A.; Menning, C. A.; Neuenswander, S. A.; Sengupta, S. K.; Thapa, P. S.; Ritter, J. C. A Mechanistic Study of Polyol Hydrodeoxygenation over a Bifunctional Pt-WOx/TiO2 Catalyst. *ACS Catal.* **2020**, *10* (21), 12996−13007.
(23) Wang, T.; Tamura, M.; Nakagawa, Y.; Tomishige, K. Preparation of Highly Active Monometallic Rhenium Catalysts for Selective Synthesis of 1,4-Butanediol from 1,4-Anhydroerythritol. *ChemSusChem* **2019**, *12* (15), 3615−3626.
(24) Virgilio, E. M.; Padró, C. L.; Sad, M. E. Effect of Support Properties on Selective Butanediols Production from Erythritol using Ir/ReOx Catalysts. *ChemCatChem.* **2021**, *13* (17), 3889−3906.
(25) MacQueen, B.; Barrow, E.; Rivera Castro, G.; Pagan-Torres, Y.; Heyden, A.; Lauterbach, J. Optimum Reaction Conditions for 1,4-Anhydroerythritol and Xylitol Hydrodeoxygenation over a ReOx−Pd/CeO2 Catalyst via Design of Experiments. *Ind. Eng. Chem. Res.* **2019**, *58* (20), 8681−8689.
(26) MacQueen, B.; Royko, M.; Crandall, B. S.; Heyden, A.; Pagán-Torres, Y. J.; Lauterbach, J. Kinetics Study of the Hydrodeoxygenation of Xylitol over a ReOx-Pd/CeO2 Catalyst. *Catalysts* **2021**, *11* (1), 108.
(27) Chia, M.; Pagán-Torres, Y. J.; Hibbitts, D.; Tan, Q.; Pham, H. N.; Datye, A. K.; Neurock, M.; Davis, R. J.; Dumesic, J. A. Selective Hydrogenolysis of Polyols and Cyclic Ethers over Bifunctional Surface Sites on Rhodium−Rhenium Catalysts. *J. Am. Chem. Soc.* **2011**, *133* (32), 12675−12689.
(28) Xi, Y.; Lauterbach, J.; Pagan-Torres, Y.; Heyden, A. Deoxydehydration of 1,4-anhydroerythritol over anatase TiO2 (101)-supported ReOx and MoOx. *Catal. Sci. Technol.* **2020**, *10*, 3731−3738.
(29) MacQueen, B.; Ruiz-Yi, B.; Royko, M.; Heyden, A.; Pagan-Torres, Y. J.; Williams, C.; Lauterbach, J. In-Situ Oxygen Isotopic Exchange Vibrational Spectroscopy of Rhenium Oxide Surface Structures on Cerium Oxide. *J. Phys. Chem. C* **2020**, *124* (13), 7174−7181.
(30) Vesborg, P. C. K.; Jaramillo, T. F. Addressing the terawatt challenge: scalability in the supply of chemical elements for renewable energy. *RSC Adv.* **2012**, *2* (21), 7933−7947.
(31) Sandbrink, L.; Beckerle, K.; Meiners, I.; Liffmann, R.; Rahimi, K.; Okuda, J.; Palkovits, R. Supported Molybdenum Catalysts for the Deoxydehydration of 1,4-Anhydroerythritol into 2,5-Dihydrofuran. *ChemSusChem* **2017**, *10*, 1375−1379.
(32) Dethlefsen, J. R.; Lupp, D.; Oh, B.-C.; Fristrup, P. Molybdenum-Catalyzed Deoxydehydration of Vicinal Diols. *ChemSusChem* **2014**, *7* (2), 425−428.
(33) Nacy, A.; Lima e Freitas, L. F.; Albarracín-Suazo, S.; Ruiz-Valentín, G.; Roberts, C. A.; Nikolla, E.; Pagán-Torres, Y. J. Selective C−O Bond Cleavage of Bio-Based Organic Acids over Palladium Promoted MoOx/TiO2. *ChemCatChem.* **2021**, *13* (5), 1294−1298.
(34) Liu, L.; Asano, T.; Nakagawa, Y.; Tamura, M.; Tomishige, K. One-pot synthesis of 1,3-butanediol by 1,4-anhydroerythritol hydrogenolysis over a tungsten-modified platinum on silica catalyst. *Green Chem.* **2020**, *22* (8), 2375−2380.
(35) Chia, M.; Haider, M. A.; Pollock, G.; Kraus, G. A.; Neurock, M.; Dumesic, J. A. Mechanistic Insights into Ring-Opening and Decarboxylation of 2-Pyrones in Liquid Water and Tetrahydrofuran. *J. Am. Chem. Soc.* **2013**, *135* (15), 5699−5708.
(36) Karim, W.; Spreafico, C.; Kleibert, A.; Gobrecht, J.; VandeVondele, J.; Ekinci, Y.; van Bokhoven, J. A. Catalyst support effects on hydrogen spillover. *Nature* **2017**, *541* (7635), 68−71.
(37) Shetty, M.; Murugappan, K.; Green, W. H.; Román-Leshkov, Y. Structural Properties and Reactivity Trends of Molybdenum Oxide Catalysts Supported on Zirconia for the Hydrodeoxygenation of Anisole. *ACS Sustainable Chem. Eng.* **2017**, *5* (6), 5293−5301.
(38) Nakagawa, Y.; Tazawa, S.; Wang, T.; Tamura, M.; Hiyoshi, N.; Okumura, K.; Tomishige, K. Mechanistic Study of Hydrogen-Driven Deoxydehydration over Ceria-Supported Rhenium Catalyst Promoted by Au Nanoparticles. *ACS Catal.* **2018**, *8* (1), 584−595.
(39) Raju, S.; Moret, M.-E.; Klein Gebbink, R. J. M. Rhenium-Catalyzed Dehydration and Deoxydehydration of Alcohols and Polyols: Opportunities for the Formation of Olefins from Biomass. *ACS Catal.* **2015**, *5* (1), 281−300.
(40) Sadeghmoghaddam, E.; Gu, H.; Shon, Y.-S. Pd Nanoparticle-Catalyzed Isomerization vs Hydrogenation of Allyl Alcohol: Solvent-Dependent Regioselectivity. *ACS Catal.* **2012**, *2* (9), 1838−1845.
(41) Yin, H.; Wada, Y.; Kitamura, T.; Kambe, S.; Murasawa, S.; Mori, H.; Sakata, T.; Yanagida, S. Hydrothermal synthesis of

https://doi.org/10.1021/acssuschemeng.1c06877
ACS Sustainable Chem. Eng. XXXX, XXX, XXX−XXX

nanosized anatase and rutile TiO2 using amorphous phase TiO2. *J. Mater. Chem.* **2001**, *11* (6), 1694−1703.
(42) Tsilomelekis, G.; Boghosian, S. On the configuration, molecular structure and vibrational properties of MoOx sites on alumina, zirconia, titania and silica. *Catal. Sci. Technol.* **2013**, *3*, 1869−1888.
(43) Zhu, H.; Shen, M.; Wu, Y.; Li, X.; Hong, J.; Liu, B.; Wu, X.; Dong, L.; Chen, Y. Dispersion Behaviors of Molybdena on Titania (Rutile and/or Anatase). *J. Phys. Chem. B* **2005**, *109* (23), 11720−11726.
(44) Hu, H.; Wachs, I. E.; Bare, S. R. Surface Structures of Supported Molybdenum Oxide Catalysts: Characterization by Raman and Mo L3-Edge XANES. *J. Phys. Chem.* **1995**, *99* (27), 10897−10910.
(45) Suarez, W.; Dumesic, J. A.; Hill, C. G. Acidic properties of molybdena-alumina for different extents of reduction: Infrared and gravimetric studies of adsorbed pyridine. *J. Catal.* **1985**, *94*, 408−421.
(46) Falcone, D. D.; Hack, J. H.; Klyushin, A. Y.; Knop-Gericke, A.; Schlögl, R.; Davis, R. J. Evidence for the Bifunctional Nature of Pt-Re Catalysts for Selective Glycerol Hydrogenolysis. *ACS Catal.* **2015**, *5* (10), 5679−5695.
(47) Lei, N.; Zhao, X.; Hou, B.; Yang, M.; Zhou, M.; Liu, F.; Wang, A.; Zhang, T. Effective Hydrogenolysis of Glycerol to 1,3-Propanediol over Metal-Acid Concerted Pt/WOx/Al2O3 Catalysts. *ChemCatChem.* **2019**, *11* (16), 3903−3912.

https://doi.org/10.1021/acssuschemeng.1c06877
ACS Sustainable Chem. Eng. XXXX, XXX, XXX−XXX